Comprehensive X-ray photoelectron spectroscopy study of the conversion reaction mechanism of CuO in lithiated thin film electrodes

Lucile Martin, Hervé Martinez, Delphine Poinot, Brigitte Pecquenard, Frédéric Le Cras

Comprehensive X-ray Photoelectron Spectroscopy Study of the Conversion Reaction Mechanism of CuO in Lithiated Thin Film Electrodes

Lucile Martin,[†,‡] Hervé Martinez,[*,†] Delphine Poinot,[‡,§] Brigitte Pecquenard,[§] and Frédéric Le Cras[‡]

[†]IPREM ECP – UMR5254, Université de Pau et des Pays de l'Adour, Hélioparc Pau-Pyrénées, 2 Av du Président Pierre Angot, 64053 Pau Cedex 9, France

[‡]CEA LITEN, 17 Rue des Martyrs, 38054 Grenoble, France

[§]CNRS ICMCB site de l'ENSCBP, Université de Bordeaux, 87 Av du Dr. Schweitzer, 33608 Pessac Cedex, France

ABSTRACT: The course of the conversion reaction during the electrochemical insertion/deinsertion of lithium in CuO thin film electrodes was surveyed by cyclic voltammetry (CV) and X-ray photoelectron spectroscopy (XPS). The electrochemical processes were studied through the comprehensive acquisition and interpretation of XPS and Auger spectra (Cu 2p, O 1s, Cu LMM) recorded at different stages of the first cycle of a Li/CuO cell. The reduction process consisting of three main steps leads successively to Cu^{+} and Cu^{0} and involves a Li_2O_2 peroxide type phase as an intermediate, whereas Li_2O is the main lithiated oxide at the end of the discharge. Only the two last steps appear reversible in charge. No evidence of Cu^{2+} was found at the end of the charge at 3.5 V/Li^{+}/Li, showing the irreversibility of the first step in our experimental conditions. Complementary XPS depth profile analyses were performed to check the evolution of the active material composition over the thickness of the electrode.

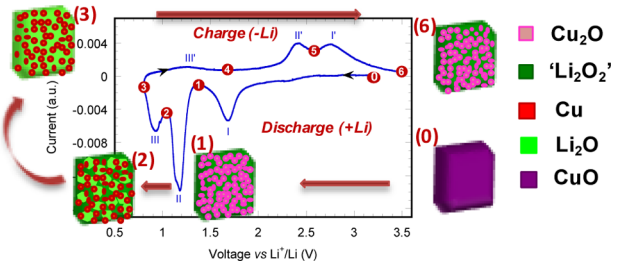

INTRODUCTION

The positive electrode active materials used in secondary lithium batteries available on the market are typically intercalation compounds. Indeed, the intercalation/deintercalation process offers the advantages to be fully reversible and to occur with a low polarization between the charge and the discharge. Nevertheless, as the capacity associated with these reactions depends on the number of available sites for lithium ions in the crystal structure, it is generally limited to less than one Li per transition metal present in the intercalation compound. Far better capacities are delivered by lithium primary batteries. Here, the lithium insertion was supposed to be irreversible as it leads to a deep transformation of the cathode material structure (in particular MX_y: M = Fe, Cu, Ag, V, ...; X = O, S), accompanied by the reduction of the transition metal and possibly the anion through several oxidation states. Tarascon et al.[1] first reported the reversibility of the conversion reaction ($MO_x + 2xLi \leftrightarrow M + xLi_2O$) in nanometer-sized 3d transition metal (Fe, Co, Ni, Cu, ...) oxides. Then, in the last ten years, numerous studies were devoted to conversion materials.[2,3]

Among these transition metal oxides, CuO is an attractive material for all-solid-state microbattery applications because of its high theoretical specific capacities (674 mAh g^{-1} and 4260 mAh cm^{-3}), its operating voltage between 1.4 and 1.0 V,[4] and its ability to be easily prepared in a thin film form by sputtering. In this case, a reversible behavior is expected due to the reduced thickness of the film. Indeed, since Tarascon et al. first reported the reversible lithium conversion reactivity of CuO particles,[5,6] various nanostructured CuO materials were synthesized as electrodes for Li-ion batteries which exhibit higher electrochemical performances compared to bulk CuO. The advantages of nanomaterials essentially lie in their shorter diffusion path for both electrons and lithium ions, larger electrode–electrolyte contact area, and a better accommodation for the strain caused by lithium insertion/deinsertion than those of conventional electrode materials.[7,8] Nanostructured films with different architectures were studied such as flower-like film, nanotube film, and nanoribbon arrays.[9−11] Feng et al.[12] have recently reported that CuO nanocrystal film elaborated by room-temperature sputtering exhibits a high reversible capacity of 570 mAh g^{-1} over 50 cycles with 97% capacity retention. Moreover, Ke et al.[11] have attributed the excellent cycleability, the high capacity retention, and the high rate capability of their CuO nanoribbon array electrode to its peculiar large surface area nanostructure, numerous interspaces between CuO nanoribbons, and a strong adhesion to the Cu current collector. Although various novel CuO nanostructures were reported as electrodes for Li-ion batteries,[13−15] the interpretation of the shape of the different voltage curves is always based on the

mechanisms proposed by Tarascon et al.,[6] which remains the sole study regarding the Li insertion processes occurring in CuO nanomaterials.

This paper reports on a thorough study by X-ray photoelectron spectroscopy (XPS) of the redox mechanisms occurring during lithium insertion/deinsertion into CuO thin film. This configuration allows getting more direct information on the Li reaction mechanisms, as parasitic reactions or limitations due to binders or conducting additive materials are excluded. This study was carried out by XPS to follow step by step the conversion processes in lithiated CuO thin film electrodes. XPS is actually a powerful tool to obtain an accurate understanding of the electrochemical reaction during cycling. This technique has the capability to observe the changes of the local environment and oxidation states of the atoms at different charge and/or discharge depths. It was successfully used to characterize the electrochemical behavior of various thin film electrodes such as V_2O_5 and TiO_yS_z.[16,17] XPS analyses of CuO thin films were performed at different discharge/charge potentials of the first cycle. Even if the formation of a solid electrolyte interphase (SEI) was clearly evidenced on these thin films over cycling, this study is only devoted to the redox processes occurring in CuO for the sake of clarity. Correlations were established between the chemical composition of the active lithiated material determined by XPS analysis (achieved after erosion to remove the SEI) and specific capacities measured during the first electrochemical cycle. A comparison was done between the Li^+ ion content determined from the specific capacities and the Li^+ ion content estimated from the XPS data.

EXPERIMENTAL SECTION

CuO Thin Film Preparation. CuO thin films were prepared by reactive radio frequency magnetron sputtering using a copper target in (Ar + O_2) atmosphere (Plassys MP700 device). All the stainless steel substrates were first cleaned by isopropanol vapor before their introduction in the deposition chamber. Before deposition, the substrates were also etched by argon ions using an ion beam, and then the target was presputtered during 15 min in the Ar−O_2 atmosphere. During the deposition, the power density applied to the target was fixed to 2.3 W cm^{-2}, and the total flow rate was kept at 50 sccm and the oxygen flow rate at 6 sccm. A total pressure of 1 Pa was applied, and the substrate holder was rotating to get homogeneous thin films. The substrates were not heated intentionally.

SEM Analysis. The cross-section and surface morphologies of thin films were observed by scanning electron microscopy using a Jeol 6700-F microscope. To avoid any charge effects on the samples, the films were systematically coated with a thin gold film.

Electrochemical Measurements. Electrochemical characterizations were performed in CR2032-type coin cells containing the CuO working electrode. The mass of each CuO thin film (ca. 400 μg) was precisely measured with a microbalance before coin cell assembly. A lithium foil (Chemetall) was used as the negative electrode. The electrolyte was 1 M $LiPF_6$ in a 1:1:3 volumetric mixture of ethylene carbonate (EC), propylene carbonate (PC), and dimethyl carbonate (DMC), with 2 wt % of vinylene carbonate (VC) (Novolyte). A polypropylene microporous membrane (Celgard 2400) associated with a nonwoven polypropylene felt (Viledon, Freudenberg) was used as a separator. Cyclic voltammetry was carried out on a VMP galvanostat/potentiostat (Bio-Logic) at 20 °C and at a scan rate of 5 μV s^{-1}. All Li_xCuO electrodes were extracted from the cell and then washed with fresh DMC to remove residual electrolyte solvents and salt. The Li content (x) was determined from specific capacities with a typical deviation of 10%. Cell assembly, disassembly, and electrode washing processes were carried out in an argon-filled glovebox. Samples were packaged in airtight glass tubes under argon and introduced in the glovebox connected to the XPS spectrometer.

XPS Analysis. X-ray photoelectron spectroscopy (XPS) measurements were carried out with a Thermo K-alpha spectrometer using a microfocused monochromatized Al Kα radiation (hν = 1486.7 eV). The XPS spectrometer was directly connected to an argon drybox to avoid any moisture and air exposure of the samples. The residual pressure inside the analysis chamber was 1×10^{-9} mbar. The spectrometer was calibrated using the photoemission lines of Ag $3d_{5/2}$, Au $4f_{7/2}$, and Cu $2p_{3/2}$. The peaks were recorded with constant pass energy of 30 eV. The diameter of the irradiated area of the sample was 400 μm. Charging effects were minimized by the use of a dual beam charge neutralization system which combines low energy electrons and Ar^+ ions to provide efficient charge compensation. To check that the sample was not reduced or damaged by X-rays, one scan per element was collected before and after XPS core peak acquisition performed on a sample. The Casa software was used to fit photoelectron spectra using a least-squares algorithm. The background in narrow range spectra was accommodated by a nonlinear Shirley function.[18] The experimental curves were fitted using combinations of Gaussian (70%) and Lorentzian (30%) distributions determined with respect to reference compounds. As all the phases were not sufficiently good conductors to preclude charging effects, the binding energy (BE) scale was calibrated from the hydrocarbon contamination using the C 1s peak at 285.0 eV. For some samples, different charging effects were observed for the different coexisting phases. In this specific case, some components of a core peak have to be calibrated, whereas some components are not affected by charging effects; thus, their binding energies were obtained directly without any calibration (for copper compounds for example). Quantification was performed on the basis of Scofield's relative sensitivity factors.[19]

All the XPS analyses were performed on cycled CuO thin films after mechanical erosion to remove the passivation layer covering the electrode surface and to efficiently probe the electrochemical mechanisms occurring inside the thin film during cycling. This type of removed-matter technique is the less damaging in terms of species transformation and was successfully used in our group in several studies on V_2O_5 or TiO_yS_z thin films for example.[16,17] Note that the mechanical erosion performed with a scalpel blade under ultrahigh vacuum in the transfer chamber or under argon in the drybox connected to the XPS spectrometer leads to the same XPS results.

RESULTS

XPS Analysis on Copper References: Cu, Cu_2O, and CuO. A detailed XPS analysis of the different core peaks (Cu 2p and O 1s) and Auger spectrum is required to characterize the three different copper reference samples (Cu, Cu_2O, and CuO). Indeed, according to the literature, these compounds present a nearly identical binding energy for their main Cu 2p core peaks (Cu $2p_{3/2}$ binding energies are, respectively, equal to 932.3 and 932.4 eV for Cu and Cu_2O).[20] Furthermore, previous

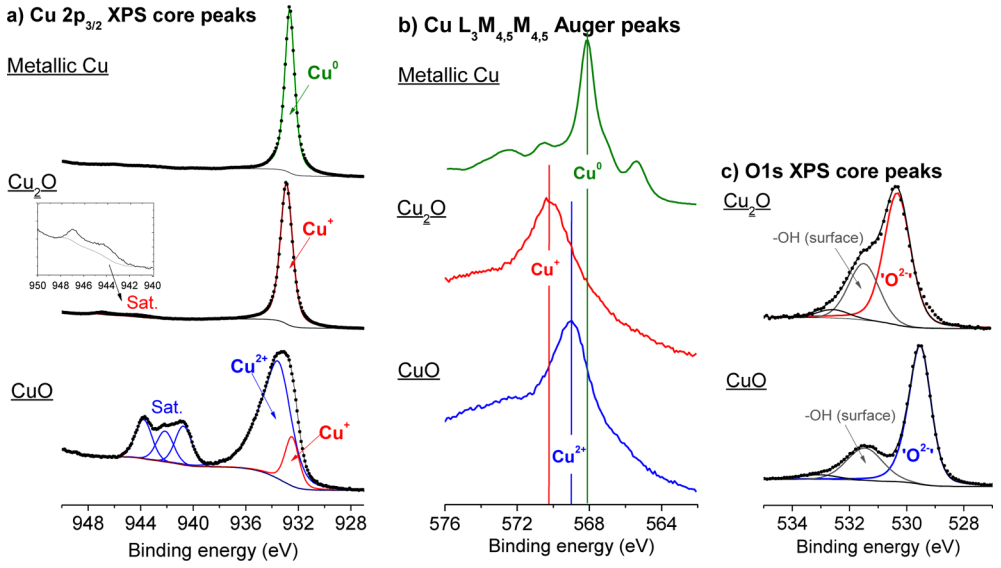

Figure 1. XPS spectra (Cu $2p_{3/2}$ and O 1s core peaks) and Auger spectra (Cu $L_3M_{4,5}M_{4,5}$ peak) of the Cu, Cu_2O, and CuO references. Cu_2O and CuO samples are thin films elaborated by RF magnetron sputtering, while the Cu sample is a foil etched before the XPS analysis to fully remove the surface oxide layer.

XPS studies have demonstrated that the energy shift of the Cu Auger peak is a good fingerprint of the copper oxidation state.[21,22]

The Cu $2p_{3/2}$ core peaks obtained for the Cu, Cu_2O, and CuO references are presented in Figure 1a. The Cu $2p_{3/2}$ signal is stable during the XPS analysis which indicates that no reduction of copper oxides takes place under the X-ray beam. For metallic copper and Cu_2O standard samples, the $Cu2p_{3/2}$ analysis, respectively, reveals the presence of a peak located at 932.6 and 932.8 eV confirming that these two compounds cannot be precisely differentiated by their Cu 2p core peak position. Nevertheless, a slight difference in the Cu 2p signature is observed as very weak satellite peaks are detected for the Cu_2O sample at higher binding energies, between 942.0 and 948.0 eV, while no satellite structure is observed for metallic copper. Harmer et al.[23] previously reported the presence of these weak excited final state satellites in the Cu 2p core peak spectrum of the Cu_2O compound and suggested that they could be associated with minor contributions from Cu d^9 initial state configurations. Moreover, note that a Gaussian−Lorentzian sum SGL(p) with Lorentzian character 'p' of 30 gives better fits on the low binding energy side for copper oxides than the more usual product GL(p), which is in agreement with the conclusion of these last authors.

For the CuO sample, the main $2p_{3/2}$ peak presents two components: the main one located at 933.6 eV is assigned to Cu(II) ions characteristic of the CuO phase, and the low intensity one (932.8 eV) corresponds to Cu(I) ions (10% of the total copper content). This last XPS result is directly in agreement with the XRD data showing that impurities of Cu_2O are present in the as-prepared CuO thin film. Moreover, some CuO nanopowders and thin films exhibit room-temperature ferromagnetism (FM) depending upon the oxygen vacancy concentration at the surface.[24,25] Indeed, Gao et al.[24] have shown that a few percent of Cu(I) ions is trapped in their CuO samples from a Cu $2p_{3/2}$ XPS core peak analysis. The other XPS peaks of the Cu $2p_{3/2}$ signal, located at higher binding energies, can be attributed to satellite peaks (940−945 eV). According to the literature,[26,27] the detection of two well-separated lines (main line at 933.6 eV and satellite line in the range of 940−945 eV) can be interpreted by the occurrence of two different final states for CuO: the $3d^{10}L^{-1}$ configuration (ligand-to-metal charge transfer during the photoemission process) and the $3d^9L$ configuration (the same as the initial state). The main asymmetric line has no splitting and is therefore ascribed to a $3d^{10}L^{-1}$ valence-band configuration as the 3d shell of the ionized copper atom is completely filled. The satellite line is rather structured, and at least three components can be observed (940.8, 942.3, and 943.9 eV), and is assigned to the $3d^9L$ configuration. For this last assignment, the 3d shell of the ionized copper is partially filled, and the open 2p and 3d shells will give rise to multiplet-split final states. Finally, the Cu $2p_{3/2}$ signature of CuO is well different from that of Cu_2O and Cu, as intense satellite peaks at ca. 6 eV above the main line are characteristic of Cu(II) in an oxygen environment.

Auger electrons are also created under X-ray radiation, and the examination of Auger energy level may be useful to identify the signature of a specific oxidation state, especially when the chemical shift of an element presents only few variations. For these specific elements, the Auger process, which has a two-hole final state, could be more strongly affected by extra-atomic relaxation than the one-hole final state photoelectron spectra. Then, distinct changes in Auger peak shape are observed for different chemical states. Figure 1b shows the copper $L_3M_{4,5}M_{4,5}$ Auger electron spectra obtained for copper and copper oxides references. A $L_3M_{4,5}M_{4,5}$ Auger electron is created when a vacancy in the $2p_{3/2}$ level is filled by a 3d electron with simultaneous ejection of another 3d electron. We previously observed that the Cu 2p spectra are similar for Cu and Cu_2O, but their Auger spectra are different. The metallic copper Auger spectrum presents a well-resolved fine structure in agreement with Schön et al.[28] This structure is not present for the copper oxide Auger spectra. The binding energies of the main Auger peak are, respectively, measured at 568.1, 570.2, and 568.9 eV for Cu, Cu_2O, and CuO. These well-distinct binding energies thus correspond to Cu^0, Cu^+, and Cu^{2+} formal oxidation states which are reported in Figure 1b.

Concerning the analysis of the O 1s core peaks for Cu_2O and CuO references (Figure 1c), the main O 1s component has a different binding energy for the two copper oxides explained by a different Cu−O bond iono-covalency. The main O 1s component, located at 530.3 eV, arises from oxygen in the Cu_2O lattice, while the main peak present at 529.6 eV is attributed to oxygen in the CuO lattice in agreement with a previous paper.[20] For Cu_2O and CuO samples, the noticeable shoulder on the higher binding energy side, located at 531.5 eV, arises from −OH surface species (~10% in atomic percentage). This shoulder was already observed in bulk, nanostructured, and thin film copper oxides in the literature.[29,30] The weak component measured at 533.0 eV also arises from surface species and could be assigned to C−O groups. This last assignment is in agreement with the detection of a weak component located at 286.3 eV in the C 1s core peak.

The O/Cu ratio is determined by a quantitative XPS analysis (Table 1) for the CuO thin film which corresponds to the pristine electrode material. Only the area of the O 1s signal that can be assigned to O atoms bound to Cu was considered to calculate the O/Cu ratio. Several quantitative analyses performed on different CuO thin films show a systematic oxygen deficiency ($CuO_{0.9}$), in agreement with the detection of a few percent of Cu(I) ions.

Table 1. XPS Binding Energies (BEs (eV)) of Core Peaks for the Cu, Cu_2O, and CuO Reference Samples[a]

	core peaks	BE (eV) (fwhm (eV))	(%)
Cu	Cu $2p_{3/2}$	932.6 (1.0) (Cu^0)	95.4
	O 1s	531.5−532.5	1.4
	C 1s	surface contamination	3.2
Cu_2O	Cu $2p_{3/2}$	932.8 (1.1) (Cu^+)	39.8
		942.0−948.0 (sat.)	1.6
			41.4
	O 1s	530.3 (1.1) ("O^{2-}")	20.0
		531.5 (1.3) (−OH)	8.6
		533.0 (1.3) (C−O)	1.4
			30.0
	C 1s	surface contamination	28.6
CuO	Cu $2p_{3/2}$	933.6 (2.4) (Cu^{2+})	17.6
		932.7 (1.3) (Cu^+)	2.9
		940.8 (1.6), 942.3 (1.6),	-
		943.9 (1.6) (sat.)	9.1
			29.6
	O 1s	529.6 (1.0) ("O^{2-}")	26.0
		531.5 (1.6) (−OH)	12.3
		533.2 (1.6) (C−O)	1.6
			39.9
	C 1s	surface contamination	30.5

[a]The full width at half-maximum (fwhm) values are indicated between brackets. For each component of one orbital, the corresponding atomic percentage (%) is reported, and the total percentage is indicated in the last line.

Electrochemical Behavior of CuO Thin Films. The electrochemical properties of CuO thin films were investigated by cyclic voltammetry experiments in the 0.8−3.5 V vs Li^+/Li potential range. The cyclic voltammogram (CV) of the Li/CuO cell is displayed in Figure 2 and corresponds to the first cycle. Three reduction peaks are observed at 1.7, 1.2, and 0.9 V vs Li^+/Li (Figure 2), indicating the multistep character of the electrochemical reaction of the CuO thin film with lithium. For tailor-made CuO particles, Debart et al.[6] observed an electrochemical plateau around 1.6 V vs Li^+/Li in their voltage−composition curve, which was attributed to the electrochemically driven CuO → Cu_2O phase transition with the concomitant formation of the unidentified amorphous lithiated phase. The above-cited authors also observed a second well-defined plateau at 1.3 V vs Li^+/Li which was ascribed to the full transformation of the intermediate Cu_2O phase into metallic copper nanoparticles embedded in a Li_2O matrix.

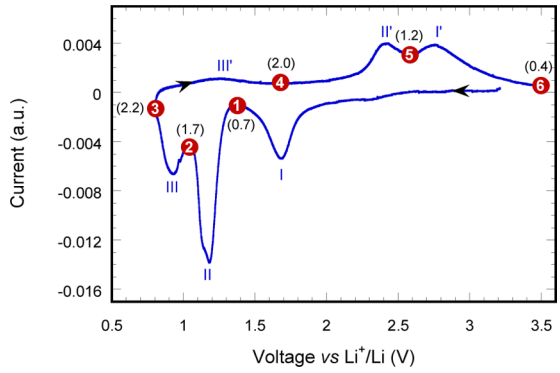

Figure 2. Voltammogram of the first cycle of a Li/CuO cell performed between 0.8 and 3.5 V at a scan rate of 5.0 $\mu V\ s^{-1}$. The dots indicate the samples studied by XPS at different stages of the first cycle, with their corresponding Li_xCuO overall composition (x values) between brackets.

During the charge, a weak oxidation peak is observed at 1.3 V vs Li^+/Li, and at least two other main peaks are observed around 2.4 and at 2.8 V vs Li^+/Li. A similar electrochemical voltammogram was obtained for CuO nanorods by Gao et al.[13]

During the first discharge process, the capacity is close to the theoretical one corresponding to 2.0 Li^+ ions inserted per CuO unit formula. Subsequently, the sum of the electrochemical processes which take place during the discharge is not totally reversible as 0.4 Li^+ ions are not extracted from the thin film at the end of the first charge.

XPS Analysis: Redox Processes Occurring during the First Cycle. To study the reduction/oxidation mechanisms involved during the reaction of Li with a CuO thin film electrode, the Cu $2p_{3/2}$ XPS core peaks, the Cu $L_3M_{4,5}M_{4,5}$ Auger spectra, and the O 1s XPS core peaks were recorded at different stages of the first cycle and are presented in Figures 3 and 4.

Cu $2p_{3/2}$ XPS Core Peaks and Cu $L_3M_{4,5}M_{4,5}$ Auger Spectra Analysis. The Cu $2p_{3/2}$ core peaks corresponding to the CuO thin film electrodes at different discharge/charge potentials are displayed in Figure 3a. After discharge down to 1.4 V/Li^+/Li (point 1), the intense satellites of CuO disappear on the Cu $2p_{3/2}$ spectrum, and the main peak shifts to a lower binding energy (932.7 eV). This evolution is consistent with the reduction of CuO into Cu_2O and/or Cu. The complementary Auger spectrum analysis allows the distinction between +1 and 0 copper oxidation states (Figure 3b). The initial $L_3M_{4,5}M_{4,5}$ Auger peak located at 568.9 eV and characteristic of Cu^{2+} oxidation state has disappeared at point 1, while two new components are observed at 568.1 and 570.3 eV, with similar intensities. This reveals that the initial Cu^{2+} oxidation state characteristic of the CuO starting material is reduced into a mixing of Cu^+ and Cu^0 oxidation states from the first step of the discharge.

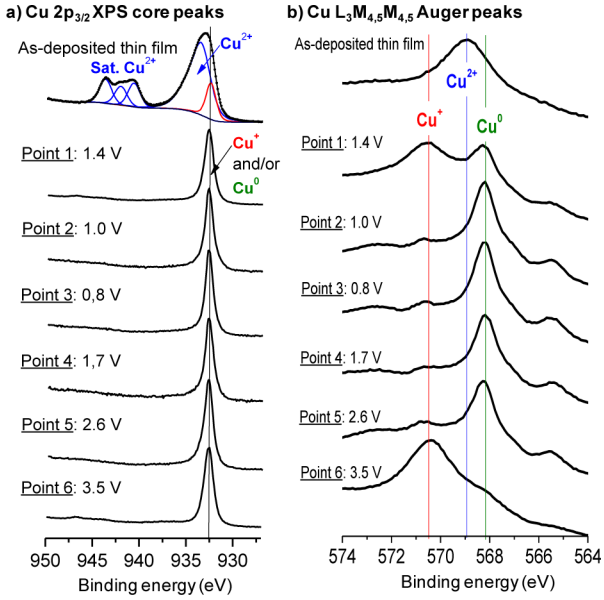

Figure 3. XPS analyses of (a) Cu $2p_{3/2}$ XPS core peak and (b) Cu $L_3M_{4,5}M_{4,5}$ Auger peak performed onto cycled CuO thin film electrodes at different stages of the first cycle: the as-deposited thin film, upon discharge (points 1, 2, and 3) and during the charge (points 4, 5, and 6).

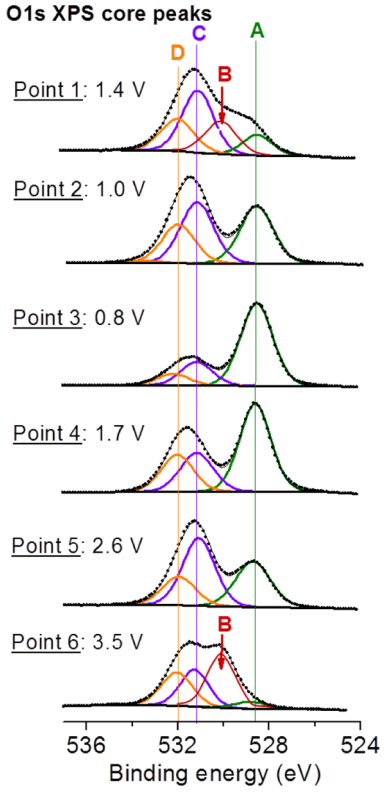

Figure 4. XPS analyses of the O 1s core peak performed onto lithiated CuO thin film electrodes at different stages of the first cycle: upon discharge (points 1, 2, and 3) and during the charge (points 4, 5, and 6).

Then, after the second step of the discharge (point 2, 1.0 V/Li^+/Li), the Auger spectrum consists of an intense peak at 568.1 eV, and the well-resolved fine structure is typical of metallic copper. This Cu^0 oxidation state is preserved until the end of the reduction process (point 3, 0.8 V/Li^+/Li).

At the beginning of the first charge (points 4 and 5), the Auger spectra remain similar to the previous one (point 3). This seems to indicate that no reoxidation of the copper occurs before 2.6 V/Li^+/Li in charge. At the end of the first charge (point 6, 3.5 V/Li^+/Li), the intensity of the component located at 568.1 eV has greatly decreased, and the main component is now located at 570.3 eV, indicating the coexistence of Cu^0 and Cu^+ oxidation states, Cu^+ ions being the majority species. The absence of Cu^{2+} oxidation state is confirmed on both the Auger and $Cu2p_{3/2}$ XPS core peak spectra (Figure 3a, point 6) for which no satellite line characteristic of CuO is observed.

O 1s XPS Core Peaks Analysis. The O 1s core peak spectra are displayed in Figure 4, and the corresponding data are presented in Table 2. After discharge down to 1.4 V/Li^+/Li (point 1), the O 1s core peak was fitted into four components (from A to D), and we can first notice that the component of O^{2-} anions in the initial CuO network (529.6 eV) has disappeared (see Figure 1c, O 1s core peak of CuO thin film before cycling). The reduction of the CuO compound into others copper species at point 1 is in agreement with the previous results obtained from Cu 2p core peak analysis.

The first new component A, located at 528.7 eV, is characteristic of O^{2-} anions contained in a Li_2O phase.[31] As expected, the Li_2O phase which was often identified during the conversion process of transition metal oxides is also detected here.

The component B recorded at 530.1 eV is characteristic of oxygen ions in a Cu_2O-type environment in agreement with the result deduced from $L_3M_{4,5}M_{4,5}$ Auger spectrum analysis indicating the presence of a Cu^+ oxidation state in the thin film at point 1.

The component C located at 531.1 eV is more difficult to ascribe. Since this binding energy position is characteristic of O^- and/or OH^- ions,[32] the component can be assigned to lithium hydroxide (LiOH) and/or lithium peroxide (Li_2O_2) species. This issue will be discussed more in detail in the following section.

The last peak D present at 532.0 eV is associated with CO_3^{2-} like oxygen environment often present in SEI species like Li_2CO_3 and alkyl carbonates RCH_2OCO_2Li.[33] The detection of CO_3^{2-} groups is in agreement with a component located at 290.1 eV in the corresponding C 1s core peak spectrum (Table 2). These species resulting from the reduction of organic solvents contained in the electrolyte are formed at the electrode surface but can still be detected by XPS either because the mechanical erosion process is not efficient enough or because a part of these species is trapped inside voids of the electrode thin film (Figure 5).

After a discharge down to 1.0 V/Li^+/Li (point 2) and until the end of the first discharge (point 3), copper is only present in its Cu^0 oxidation state based on the analyses of the Cu LMM Auger peak and O 1s core peak for which component B assigned to Cu_2O has disappeared. Table 2 displays the quantitative XPS results obtained for the cycled CuO thin film electrodes. We can observe that the total reduction of copper oxide into metallic copper is accompanied by the increase of Li_2O (component A) atomic percentage from 3.8% to 21.7%. In the same time, the atomic percentage related to component C (O^-/OH^- ions) decreases from 12.0% to 6.2%.

During the charge process, the reverse phenomena occur as the Li_2O (component A) content decreases from 21.7% to

Table 2. Quantitative XPS Analyses Performed onto Cycled CuO Thin Film Electrodes at Different Stages of the First Cycle: Upon Discharge (Points 1, 2, and 3) and during the Charge (Points 4, 5, and 6)[a]

core peaks	Point 1: 1.4 V	Point 2: 1.0 V	Point 3: 0.8 V	Point 4: 1.7 V	Point 5: 2.6 V	Point 6: 3.5 V
BE (eV) (fwhm (eV))	Atomic Percentage (%)					
Cu $2p_{3/2}$						
932.7 (1.2) (Cu^0 and/or Cu^+)	32.6	18.2	18.8	14.3	22.5	33.9
O 1s						
A: 528.7 (1.6) ("O^{2-}" in Li_2O)	3.8	13.0	21.7	18.0	11.8	2.1
B: 530.1 (1.6) ("O^{2-}" in Cu_2O)	9.1	-	-	-	-	14.6
C: 531.1 (1.6) ("O^-"/"OH^-")	12.0	13.8	6.2	8.4	16.2	10.2
D: 532.0 (1.6) (CO_3^{2-})	6.4	9.3	3.1	7.8	7.0	10.2
Li 1s						
54.0 (1.8)−55.5 (1.8)	32.7	38.1	48.3	47.6	38.4	22.9
C 1s						
285.0 (1.6) (C−C, C−H)	1.2	1.5	0.9	1.4	1.4	2.1
290.1 (1.6) (CO_3^{2-})	2.2	2.8	1.0	2.5	2.2	4.0
F 1s						
685.0 (1.8) (LiF)	-	3.3	-	-	0.5	-

[a]XPS binding energies (BE (eV)) of core peaks are reported in the first column with the full width at half-maximum (fwhm) values between brackets. Atomic percentages corresponding to the different components of each XPS core peak are reported for the different analysis points (from 1 to 6). Note that a very small atomic percentage of fluorine (relative BE corresponding to LiF which comes from the decomposition of $LiPF_6$ electrolyte salt) was revealed by XPS analyses due to the presence of SEI traces.

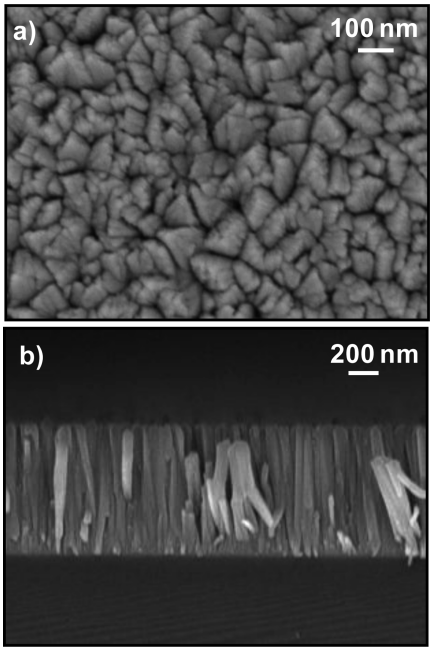

Figure 5. SEM images of the pristine CuO thin film surface (a) and cross-section (b).

2.1% and the atomic percentage related to component C (O^-/OH^- ions) increases from 6.2% to 10.2% showing a transformation of the oxygenated phases. At the end of the first charge (point 6), the component B assigned to Cu_2O is detected again, which is in agreement with the previous results obtained from Cu 2p and Cu LMM Auger spectra analysis (Figure 3).

Assignment of Component C in the O 1s Core Peak. Considering the binding energy of this component, LiOH and Li_2O_2 compounds have to be considered. Two reference samples were analyzed by XPS to get accurate binding energies for O 1s and Li 1s core peaks. The XPS analysis of LiOH powder was achieved in our group in a previous work.[31] The relative O 1s and Li 1s core peaks are, respectively, located at 531.2 and 54.8 eV. To determine the binding energies characteristic of lithium peroxide, we recorded the O 1s and the Li 1s spectra of a commercial powder containing a mixture of Li_2O_2 and Li_2O phases (Figure 6). The O 1s core peak

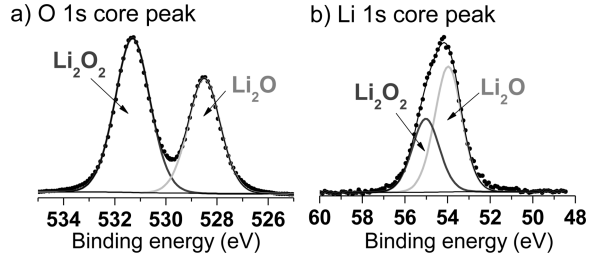

Figure 6. O 1s (a) and Li 1s (b) XPS core peak spectra of a commercial powder containing a mixture of Li_2O_2 and Li_2O compounds.

reveals two well-separated components at 528.5 and 531.3 eV, respectively, corresponding to O^{2-} and $(O_2)^{2-}$ anions related to Li_2O and Li_2O_2 phases. The Li 1s signal can be fitted with two components at 54.0 and 55.0 eV which can be assigned to Li_2O for the first one and to Li_2O_2 for the second one. The Li/O ratios estimated by quantitative XPS analysis are equal to 2.1 for Li_2O and 0.9 for Li_2O_2. These results confirm that the O 1s and Li 1s signals for LiOH and Li_2O_2 compounds cannot be separated by an XPS analysis.

However, the instability of the LiOH phase under the X-ray beam in ultrahigh vacuum is well-known and has often been observed by our group (see Supporting Information). LiOH is decomposed into Li_2O and H_2O species, this last one being desorbed. During XPS analyses of lithiated copper oxide thin films, the signature of the O 1s core peak for the first and the last scan remained the same which clearly demonstrates the stability of oxygenated phases present in the thin film under the X-ray beam. Moreover, Dedryvère et al.[31] observed the rapid decomposition of LiOH into Li_2O when an argon ion sputtering is used. Sputtering tests were thus performed on these lithiated thin films. The ratio between components.

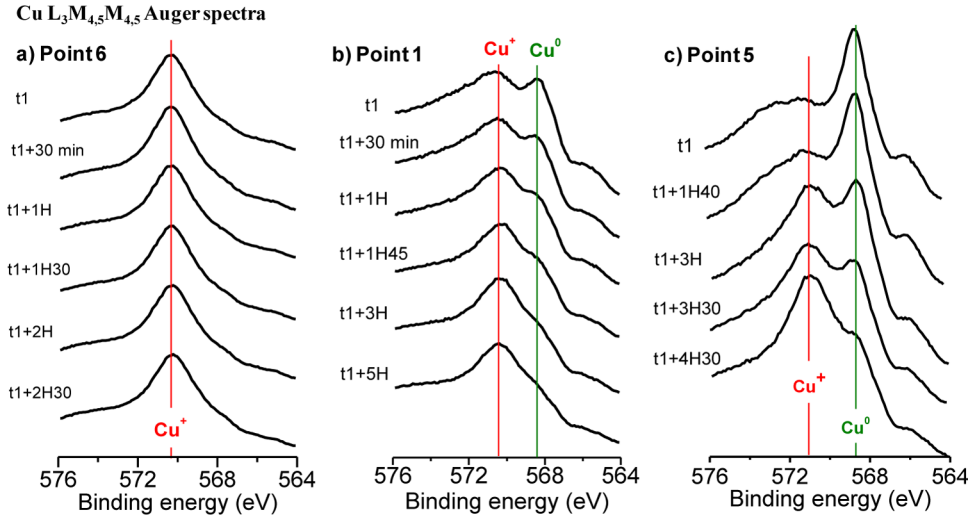

Figure 7. Depth analysis performed onto cycled CuO thin film electrodes: the Cu $L_3M_{4,5}M_{4,5}$ Auger peak was recorded at different times of an argon ion etching, and results are given for point 6 (a), point 1 (b), and point 5 (c).

$C(O^-/OH^-)$ and $A(O^{2-}(Li_2O))$ remained stable under an argon flow for more than 2 h of sputtering confirming the stability of the oxygenated phases. We can also point out that the formation of LiOH in a significant proportion inside the active thin film electrode is unlikely when aprotic solvents and high purity electrolytes are used in the cells, and drastic precautions are taken to handle and to package samples under argon in a glovebox. All these results demonstrate that the LiOH compound cannot be responsible for the presence of the intense component located at 531.1 eV for the points 1, 2, 5, and 6. We can thus deduce that this component C might be assigned to "Li_xO" species having a chemical composition close to Li_2O_2 (x is determined by quantitative XPS analyses and is close to 1). In conclusion, we have identified O^- oxygen ions in a Li^+ environment, in a ratio close to 1:1. For sake of clarity, the component C will be assigned to a Li_2O_2-type phase, noted "Li_2O_2" further in the text.

Further in-Depth XPS Analyses. Even if an intense current peak was measured at 2.4 V/Li^+/Li in charge, no reoxidation of metallic copper was observed just after this electrochemical step (Figure 3b, point 5). We can thus suppose that the copper reoxidation is not homogeneous in the thin film electrode. To check the copper oxidation state over the thickness of the lithiated thin film, an argon ion etching was used. Note that this technique has to be used very carefully because it can induce preferential sputtering of lower mass atoms and decomposition of some phases depending on the sample.[34] Soft conditions of sputtering (ion energy of 0.2 keV and low current of around 15 μA) were then applied to avoid any modifications of the sample, and tests were first performed to check the stability of the samples under argon bombardment. The etching rate calibrated on Ta_2O_5 under these conditions is equal to 0.01 nm s^{-1}. Thus, a total sputtering time of 3 h would correspond to a sputtered thickness of around 100 nm, that is to say one-quarter of the pristine CuO film thickness.

We first checked that sputtering did not induce a reduction of the copper element. In the case of point 6, where Cu^+ is present in large excess, the formal oxidation state +1 is preserved during a long etching time (more than 2 h) (Figure 7a). This result proves that no reduction of copper in its Cu^+ oxidation state takes place in our conditions of etching. Further on, the evolution of oxidation states over the thickness is characteristic of the material itself. The $L_3M_{4,5}M_{4,5}$ Auger spectra obtained for the electrodes after an etching time shorter than 60 min are similar to those obtained after a mechanical erosion for the six points studied at the first cycle. For longer time of etching (longer than 60 min), the copper oxidation state remains stable during the XPS depth profile analysis, except for points 1 and 5.

After the discharge down to 1.4 V/Li^+/Li (point 1), the thin film is more reduced near the surface with the presence of a mixture of Cu^0/Cu^+ than in the inner part where Cu^+ is mainly detected (Figure 7b). At the point 5 (2.6 V/Li^+/Li), the reoxidation of metallic copper into Cu^+ has begun in the inner layer of the thin film, while Cu^0 is still present in large excess in the upper part of the film (Figure 7 c). We checked that the evolution observed on these Cu $L_3M_{4,5}M_{4,5}$ Auger spectra is coherent with that observed on the O 1s core peaks for which we can follow modifications of the intensity of component B (530.1 eV) assigned to oxygen ions in a Cu_2O lattice.

Quantitative Analysis of the Li_2O/"Li_2O_2" Ratio and Estimation of Inserted Li Content. Quantitative XPS analysis has demonstrated that a mixture of Li_2O:"Li_2O_2" is formed after the first reduction step (Figure 8a, point 1), the oxygen relative proportions in the two phases being 1/4:3/4. We can thus estimate that 0.6 Li^+ ions per CuO unit formula are involved for the total $Cu^{2+} \rightarrow Cu^+$ reduction, as reported on Figure 8b for the value at point 1. This estimation appears in good agreement with the electrochemically measured value equal to 0.7 Li^+ ions. After discharge down to 1.0 V/Li^+/Li, the oxygen relative proportion for Li_2O:"Li_2O_2" is close to 1/2:1/2 in the thin film (Figure 8a, point 2). Considering this last result, the number of Li^+ ions inserted per CuO unit formula estimated by XPS results to 1.5 Li^+ ions per CuO unit formula, which is relatively close to the electrochemically measured value, equal to 1.7 (Figure 8b, point 2). At the end of the first discharge, the lithiated matrix now mainly consists of a Li_2O phase as the corresponding relative oxygen content in the film reaches 78% (Figure 8a, point 3).

Finally, at the end of the first charge, the amount of Li^+ ions trapped in the active material can be estimated to 0.6 per CuO unit formula, as reported on Figure 8b (point 6), considering that the remaining lithiated matrix is a mixture of Li_2O and "Li_2O_2" in a corresponding oxygen relative proportion equal to

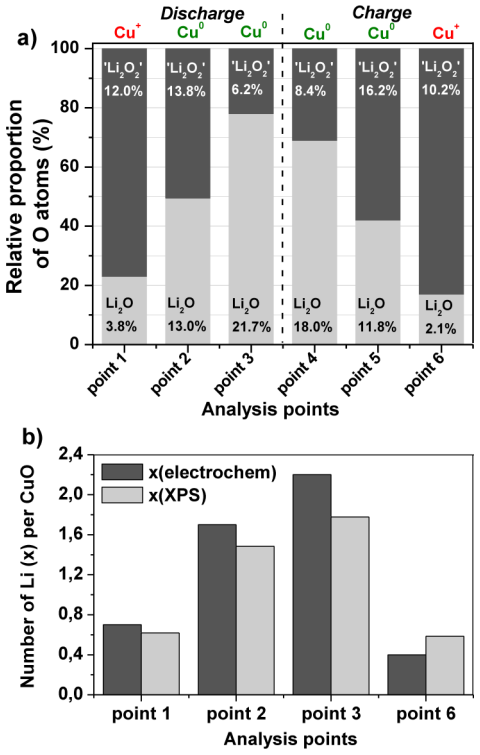

Figure 8. (a) Relative proportion of O atoms contained in Li_2O and "Li_2O_2" phases during the first cycle. The corresponding atomic concentrations are reported in histogram area for each phase (Li_2O and "Li_2O_2"). (b) Comparison between the Li^+ ion content determined from the specific capacities by electrochemical measurements and the Li^+ ion content estimated from the active material composition achieved by XPS analysis.

17%:83% (Figure 8a, point 6). This estimation is slightly higher than the measured value of 0.4 irreversible Li^+ ions.

DISCUSSION

First Discharge. Although CuO is a simple oxide, it becomes a quite complex system when lithium is inserted/deinserted. Indeed, during lithium insertion several phases are formed, and the microstructure of the electrode is evolving over cycling. In these conditions, at least three main electrochemical steps were evidenced. As expected, the two first steps, respectively, correspond to the reduction of Cu^{2+} in Cu^+ and Cu^+ into Cu^0. In the literature, the third step was attributed to the formation of a solid electrolyte interphase (SEI).

The nature of the phases formed at the end of the discharge and at the end of the charge is clearly identified. Hence, metallic copper and Li_2O are detected at the end of the discharge, while the reoxidation is only partial over the charge, leading to Cu_2O and "Li_2O_2". Cu, Li_2O, and Cu_2O were also clearly evidenced by TEM studies.[35] At the early stage of the lithium insertion, two processes can potentially occur, either an intercalation leading to a ternary phase Li−Cu−O or a conversion mechanism leading to Cu_2O and a lithiated oxide. The intercalation process was mainly evidenced for transition metal oxides where the metal has a high oxidation state. For other oxides, there is somewhat a controversy due to a competition between lithium insertion and partial conversion, and these intermediate processes may be kinetically or thermodynamically driven.[3] For CuO, the insertion of a limited amount of Li (0.4 Li/CuO) is expected around 2.2 V vs Li^+/Li, as was mentioned by Tarascon et al.[6] for nanoparticles. Although a similar process could occur in these thin film electrodes, the capacity associated with the electrochemical step I at 1.6 V/Li^+/Li (0.7 Li/CuO) is high compared to the capacity associated with the insertion process (0.4 Li/CuO) evidenced by these authors. We can note that step I is clearly located beyond the insertion region in both potential and Li content. The electrochemical reaction occurring before point 1 (step I) is then mainly attributed to an intermediate step of the conversion reaction leading to Cu_2O and "Li_2O_2". Even if it is unusual to observe oxygen anions O^- as in a peroxide phase (Li_2O_2 phase is well-known in Li-air batteries), at these potentials (close to 1.5 V) Bates et al.[4] have shown that the formation of Li_2O_2 is thermodynamically allowed. At this stage (point 1), the presence of a small amount of Cu^0 is due to a slight overlapping of electrochemical steps I and II. The depth profiling has highlighted an inhomogeneous insertion of the lithium into the thin film since Cu^+ and Cu^0 are present near the electrode/electrolyte interface while Cu^+ is mainly present in the inner part of the film. This is due to kinetic limitations and to a poor Li^+ ionic conductivity as evidenced by Xiang et al.[36] for a flower-like hierarchical CuO electrode where D_{Li+} is initially low and drastically decreases when the discharge is going on (D_{Li+} is equal to 5.05×10^{-9} cm^2 s^{-1} at the beginning of the discharge ($0 \leq x \leq 0.4$) and decreases up to 6.86×10^{-12} cm^2 s^{-1} at the end of the discharge). The second discharge step II corresponds to the total reduction of Cu^+ into Cu^0. Although, Cu^{2+} is fully reduced at point 2, an additional reaction (III) involving 0.4 Li/CuO occurs below 1 V/Li^+/Li. As mentioned previously in the literature, this step was attributed to the formation of a SEI. In a forthcoming paper, we will report others results obtained by XPS for cycled CuO thin film electrode that evidence the progressive formation of a SEI layer from the beginning of the discharge, the nature of the phases formed being potential dependent. As the Li_2O/"Li_2O_2" ratio is clearly evolving during this last reduction step III, it means that O^- species are reduced into O^{2-} anions when further Li^+ ions and electrons are inserted. The O^-/O^{2-} electrochemical couple is thus certainly involved in the overall electrochemical process. According to these results, we can propose the following mechanisms related to the three main reduction steps

Step I:

$$CuO + \mathbf{1/2Li} \rightarrow 1/2Cu_2O + 1/4\text{“}Li_2O_2\text{”}$$

Step II:

$$1/2Cu_2O + 1/4\text{“}Li_2O_2\text{”} + \mathbf{Li} \rightarrow Cu + 1/4\text{“}Li_2O_2\text{”} + 1/2Li_2O$$

Step III:

$$Cu + 1/4\text{“}Li_2O_2\text{”} + 1/2Li_2O + \mathbf{1/2Li} \rightarrow Cu + Li_2O$$

This model is quite consistent with the capacities and the compositions observed experimentally. All these mechanisms are allowed from a thermodynamic point of view, leading to a standard Gibbs free energy between −85 and −210 kJ/mol.

First Charge. At the end of the charge, the reoxidation of Cu^0 is only partial as Cu_2O is detected by XPS in large excess with a very few percent of Cu^0 and 0.4 Li^+/CuO remaining irreversibly trapped in the electrode. Note that the presence of the main copper oxide phase Cu_2O is confirmed by TEM results (not shown here). During the first step of the charge

(III′), no evolution of the oxidation state of copper is evidenced. Only 0.2 Li^+ ions were removed, indicating a weak evolution of the electrode composition associated with an oxidation of some O^{2-} anions belonging to Li_2O into O^- anions as the Li_2O:"Li_2O_2" ratio is slightly decreasing during this step III′ (Figure 8a).

The second and the third step of the charge process are not well separated (overlapping of peaks II′ and I′). The main transformation during the second electrochemical step (II′) corresponds to the consumption of Li_2O and the concomitant increase of the "Li_2O_2" content (Figure 8a, point 5). It involves 0.8 Li^+ ions per copper. These elements are in accordance with the reversal of the reaction corresponding to the reduction step III. At the end of the second step of the charge process (II′) at 2.6 V/Li^+/Li, metallic copper has started to oxidize into Cu_2O near the current collector, as shown by the depth profiling. This reaction corresponds actually to the next process occurring at higher potential and is observed at point 5 due to the overlapping of steps II′ and I′. This composition gradient indicates that the electronic transport through the electrode in its preceding state (Cu nanoparticles embedded in lithium oxides matrix) is the limiting factor of the reaction as it was previously reported by Bijani et al.[37,38] in Cu_2O micro- and nanostructured electrodeposited thin films during the charge.

Above 2.6 V/Li^+/Li, up to 0.8 Li^+ ions are extracted from the thin film during the last oxidation step (I′) which occurs in a large range of potential (from 2.6 to 3.5 V/Li^+/Li) probably due to important kinetic limitations. The corresponding reaction induces the almost full reoxidation of Cu into Cu_2O (point 6) in all the depths of the thin film, without any formation of Cu^{2+} species, and the almost full consumption of Li_2O (only 2.1 atom % left). These observations are consistent with the reversed reaction proposed for the reduction step II and with the irreversibility of the reaction proposed for the reduction step I, involving 0.5 Li/CuO, as around 0.4 Li^+/CuO are not extracted from the thin film at the end of the first charge.

The evolution of the Li_2O:"Li_2O_2" ratio reported for the first cycle in Figure 8a is quite consistent with the composition of the electrode expected from the mechanisms proposed above, as "Li_2O_2" is the majority component after step I and I′ (points 1 and 6), while Li_2O is predominant at the end of the discharge after step III (point 3), and as "Li_2O_2" and Li_2O are present in almost equal amounts after steps II and II′ (points 2 and 5).

CONCLUSION

A comprehensive study of the evolution of the Li_xCuO thin film electrode composition was achieved by X-ray photoelectron spectroscopy during a first electrochemical lithiation/delithiation cycle. The determination of the copper oxidation state, the identification of the phases formed at the successive stages of the lithium insertion/deinsertion, and the determination of their atomic concentrations allowed proposing a new mechanism for the CuO reaction with lithium. A compound with a composition and a chemical environment similar to lithium peroxide Li_2O_2, generated during an intermediate step of the conversion reaction, was highlighted for the first time in conversion reactions involving transition metal oxides. It participates in the electrochemical processes through the reversible reduction/oxidation of O^-/O^{2-} species. Both the electrochemical results and the composition depth profiles demonstrate the difficulty to sharply separate the successive intermediate transformations due to low diffusion kinetics of the different species. Finally, only two of the three main reaction steps appear to be reversible. The reoxidation of Cu_2O into CuO was not observed in our experimental conditions, possibly due to kinetics limitations amplified by the large volume change expected to occur during this step.

ASSOCIATED CONTENT

Supporting Information

XPS results showing the instability of the LiOH phase under the X-ray beam in ultrahigh vacuum. This material is available free of charge via the Internet at http://pubs.acs.org.

AUTHOR INFORMATION

Corresponding Author

*E-mail: herve.martinez@univ-pau.fr.

Notes

The authors declare no competing financial interest.

REFERENCES

(1) Poizot, P.; Laruelle, S.; Grugeon, S.; Dupont, L.; Tarascon, J.-M. *Nature* **2000**, *407*, 496−499.

(2) Malini, R.; Uma, U.; Sheela, T.; Ganesan, M.; Renganathan, N. *Ionics* **2009**, *15*, 301−307.

(3) Cabana, J.; Monconduit, L.; Larcher, D.; Palacin, M. *Adv. Mater.* **2010**, *22*, E170−E192.

(4) Bates, R.; Jumel, Y.; *Lithium Batteries*; Academic Press: London, 1983.

(5) Grugeon, S.; Laruelle, S.; Herrera-Urbina, R.; Dupont, L.; Poizot, P.; Tarascon, J.-M. *J. Electrochem. Soc.* **2001**, *148*, A285−A292.

(6) Debart, A.; Dupont, L.; Poizot, P.; Leriche, J.-B.; Tarascon, J.-M. *J. Electrochem. Soc.* **2001**, *148*, A1266−A1274.

(7) Arico, A. S.; Bruce, P.; Scrosati, B.; Tarascon, J.-M.; van Schalkwijk, W. *Nat. Mater.* **2005**, *4*, 366−377.

(8) Jamnik, J.; Maier, J. *Phys. Chem. Chem. Phys.* **2003**, *5*, 5215−5220.

(9) Pan, Q.; Jin, H.; Wang, H.; Yin, G. *Electrochim. Acta* **2007**, *53*, 951−956.

(10) Xiang, J.; Tu, J.; Huang, X.; Yang, Y. *J. Solid State Electrochem.* **2008**, *12*, 941−945.

(11) Ke, F.-S.; Huang, L.; Wei, G.-Z.; Xue, L.-J.; Li, J.-T.; Zhang, B.; Chen, S.-R.; Fan, X.-Y.; Sun, S.-G. *Electrochim. Acta* **2009**, *54*, 5825−5829.

(12) Feng, J.; Xia, H.; Lai, M.; Lu, L. *Mater. Res. Bull.* **2011**, *46*, 424−427.

(13) Gao, X.; Bao, J.; Pan, G.; Zhu, H.; Huang, P.; Wu, F.; Song, D. *J. Phys. Chem. B* **2004**, *108*, 5547−5551.

(14) Morales, J.; Sanchez, L.; Martin, F.; Ramos-Barrado, J.; Sanchez, M. *Thin Solid Films* **2005**, *474*, 133−140.

(15) Xiang, J.; Tu, J.; Zhang, L.; Zhou, Y.; Wang, X.; Shi, S. *J. Power Sources* **2010**, *195*, 313−319.

(16) Benayad, A.; Martinez, H.; Gies, A.; Pecquenard, B.; Levasseur, A.; Gonbeau, D. *J. Electron Spectrosc. Relat. Phenom.* **2006**, *150*, 1−10.

(17) Lindic, M.; Martinez, H.; Benayad, A.; Pecquenard, B.; Vinatier, P.; Levasseur, A.; Gonbeau, D. *Solid State Ionics* **2005**, *176*, 1529−1537.

(18) Shirley, D. *Phys. Rev. B: Condens. Matter Mater. Phys.* **1972**, *5*, 4709−4714.

(19) Scofield, J. *J. Electron Spectrosc. Relat. Phenom.* **1976**, *8*, 129−137.

(20) Ghijsen, J.; Tjeng, L.; Van Elp, J.; Eskes, H.; Westerink, J.; Sawatzky, G.; Czyzyk, M. *Phys. Rev. B: Condens. Matter Mater. Phys.* **1988**, *38*, 11322−11330.

(21) Timmermans, B.; Reniers, F.; Hubin, A.; Buess-Herman, C. *Appl. Surf. Sci.* **1999**, *144−145*, 54−58.

(22) Larson, P. *J. Electron Spectrosc. Relat. Phenom.* **1974**, *4*, 213−218.

(23) Harmer, S.; Skinner, W.; Buckley, A.; Fan, L.-J. *Surf. Sci.* **2009**, *603*, 537−545.

(24) Gao, D.; Zhang, J.; Zhu, J.; Qi, J.; Zhang, Z.; Sui, W.; Shi, H.; Xue, D. *Nanoscale Res.Lett.* **2010**, *5*, 769−772.

(25) Qin, H.; Zhang, Z.; Liu, X.; Zhang, Y.; Hu, J. *J. Magn. Magn. Mater.* **2010**, *322*, 1994−1998.
(26) Parmigiani, F.; Depero, L.; Minerva, T.; Torrance, J. *J. Electron Spectrosc. Relat. Phenom.* **1992**, *58*, 315−323.
(27) Parmigiani, F.; Pacchioni, G.; Illas, F.; Bagus, P. *J. Electron Spectrosc. Relat. Phenom.* **1992**, *59*, 255−269.
(28) Schön, G. *J. Electron Spectrosc. Relat. Phenom.* **1972**, *1*, 377−387.
(29) Al-Kuhaili, M. *Vacuum* **2008**, *82*, 623−629.
(30) Svintsitskiy, D.; Stadnichenko, A.; Demidov, D.; Koscheev, S.; Boronin, A. *Appl. Surf. Sci.* **2011**, *257*, 8542−8549.
(31) Dedryvere, R.; Laruelle, S.; Grugeon, S.; Poizot, P.; Gonbeau, D.; Tarascon, J.-M. *Chem. Mater.* **2004**, *16*, 1056−1061.
(32) Dupin, J.-C.; Gonbeau, D.; Vinatier, P.; Levasseur, A. *Phys. Chem. Chem. Phys.* **2000**, *2*, 1319−1324.
(33) Dedryvere, R.; Laruelle, S.; Grugeon, S.; Gireaud, L.; Tarascon, J.-M.; Gonbeau, D. *J. Electrochem. Soc.* **2005**, *152*, A689−A696.
(34) Malherbe, J.; Martinez, H.; Fernandez, B.; Pécheyran, C.; Donard, O. *Spectrochim. Acta, Part B* **2009**, *64*, 155−166.
(35) Poinot, *Ph.D. Thesis*, Bordeaux University, November 2011.
(36) Xiang, J.; Tu, J.; Qiao, Y.; Wang, X.; Zhong, J.; Zhang, D.; Gu, C. *J. Phys. Chem. C* **2011**, *115*, 2505−2513.
(37) Bijani, S.; Gabas, M.; Martinez, L.; Ramos-Barrado, J.; Morales, J.; Sanchez, L. *Thin Solid Films* **2007**, *515*, 5505−5511.
(38) Bijani, S.; Gabas, M.; Subias, G.; Garcia, J.; Sanchez, L.; Morales, J.; Martinez, L.; Ramos-Barrado, J. *J. Mater. Chem.* **2011**, *21*, 5368−5377.